Geophysical and Astrophysical Fluid Dynamics
Vol. 98, No. 1, February 2004, pp. 39–62

Taylor & Francis
Taylor & Francis Group

AN ANALYTICAL STUDY OF GENERAL HYPER-DIFFUSIVITY AND BAROTROPIC EDDIES

SANJEEVA BALASURIYA*

School of Mathematics and Statistics, University of Sydney, NSW 2006, Australia

(Received 27 December 2002; Revised 18 April 2003; In final form 30 October 2003)

An exact solution to the barotropic potential vorticity equation is used to examine the properties of barotropic vortices under arbitrary *n*th-order hyper-diffusivity. Analytical expressions are derived for an eddy's lifetime, meridional drift, decay in size, and energy, as functions of the Coriolis parameter, order and magnitude of diffusivity, and the eddy's size, shape and strength. These expressions provide a simple explanation for many observed features of oceanic and atmospheric vortices. For example, the competition between the Coriolis effect and eddy strength in giving permitted eddy geometries; the bias towards a zonal anisotropy for large vortices but not for small ones; energetic preference for axisymmetry; poleward meridional drift of cyclonic vortices; and meridional speed variation depending on eddy geometry and strength.

Keywords: Barotropic eddies; Eddy lifetime; Eddy geometry; Hyper-diffusivity; Meridional drift

1. INTRODUCTION

Oceanic and atmospheric eddies have lifetimes ranging from the infinitesimal (in turbulent flows), to several years (in Gulf Stream rings), to centuries (Jupiter's Great Red Spot); see reviews such as Richardson (1983), Provenzale (1999), Hopfinger and van Heijst (1993) or Nezlin and Snezhkin (1993). Catastrophic events such as vortex collisions obviously have an enormous effect on vortex lifetime. The influence of nearby vortices, strain fields, and diffusion also contribute towards vortex decay. An interesting question would be to attempt to quantify the role of diffusion, Coriolis effect, and eddy geometry in the lifetime expectation of an eddy. This is one issue this article will address, through an elementary model which nonetheless exactly incorporates arbitrary-order hyper-diffusivity.

Given the destructive capacities of geophysical phenomena such as tropical cyclones, there has also been considerable interest in determining the trajectories followed by eddies. A feature often observed in experimental and numerical studies is that in addition to a typical westward motion, a poleward meridional drift is to be observed in cyclones, whereas an equator-wards drift occurs in anti-cyclones. Since the initial work of Rossby (1948), many experimental (Masuda *et al.*, 1990; Carnevale *et al.*,

*E-mail: sanjeeva@maths.usyd.edu.au

ISSN 0309-1929 print: ISSN 1029-0419 online
DOI: 10.1080/03091920410001659290

1991; Stegner and Zeitlin, 1998; Flór and Eames, 2002) analytical (Adem, 1956; McWilliams and Flierl, 1979; Willoughby, 1989; Reznik, 1992; Korotaev and Fedotov, 1994; Reznik and Dewar, 1994; Llewellyn Smith, 1997) and numerical (McWilliams and Flierl, 1979; Masuda *et al.*, 1990; Smith and Ulrich, 1990; Carnevale *et al.*, 1991; Korotaev and Fedotov, 1994; Sutyrin *et al.*, 1994) studies have confirmed this observation, using many different ideas. Many of the theoretical and computational models cited are potential vorticity (PV) conserving, and use eddies with Gaussian, Rankine or singular cores (Carnevale *et al.*, 1991; Reznik, 1992; Korotaev and Fedotov, 1994; Reznik and Dewar, 1994; Sutyrin *et al.*, 1994; Llewellyn Smith, 1997). McWilliams and Flierl (1979) additionally consider frictional and baroclinic effects. The analytical hyper-diffusive model developed in the current article will also possess a poleward drift of cyclonic eddies. It will moreover obtain an exact expression for the trajectory followed by such an eddy, and its meridional drift speed. In this idealised but dynamically exact situation, the dependence of these quantities on the parameters of the situation will be obtained. The results are consistent with observations that the meridional speed increases with time (McWilliams and Flierl, 1979), and the observation in some cases that the meridional displacement tends to a finite value (Carnevale *et al.*, 1991; Korotaev and Fedotov, 1994; Llewellyn Smith, 1997; Flór and Eames, 2002).

Determining the energy associated with an eddy is an important exercise, which is often studied with turbulence in mind. The current model draws some connections with energetic observations. For example, the expectation that axisymmetric vortices would eventually dominate (McWilliams, 1984; Hopfinger and van Heijst, 1993) can be shown by examining the energy associated with this solution. The model also shows why a preference for larger-scaled coherent eddies could be expected as time progresses.

It has been known for some time that, for small wavenumbers, the energy resides mainly in the zonal velocities, whereas for higher wavenumbers, the zonal and meridional modes have approximately the same energy. Such evidence is provided from actual atmospheric data by Eliasen (1958) in his Figure 1, Baer (1972) in his Table 1, and Kao and Wendell (1970) in their Section 5. Discussions and numerics on this behaviour are also provided by Kenyon (1967) and Rhines (1975). The present model is able to provide an interesting explanation for these observations.

The evolution of barotropic eddies will be studied here using an exact analytical model in which the potential vorticity is subject to nth-order diffusivity. The emphasis will be on determining expressions for an eddy's lifetime, decay in size, and trajectory. The dependencies of these on the eddy's initial length-scale, geometry and strength, the Coriolis parameter, and the order and strength of diffusivity, will be investigated.

2. THE MODEL

In the general barotropic β-plane setting, the streamfunction $\psi(x, y, t)$ is related to the PV $q(x, y, t)$ through

$$q(x, y, t) = \nabla^2 \psi(x, y, t) + f + \beta y \tag{1}$$

where f is the planetary vorticity at a fixed latitude which is chosen to be $y = 0$, and the Coriolis parameter $\beta \geq 0$ represents its variation with latitude (Pedlosky, 1979). Here, (x, y) refer to the eastward (zonal) and northward (meridional) coordinates respectively, and t is time. In the current model, the PV shall be assumed to decay subject to arbitrary-order hyper-diffusivity, according to

$$\frac{\partial q}{\partial t} + J(\psi, q) = -\nu_n\left(-\nabla^2\right)^n q, \tag{2}$$

where the Jacobian operator J is defined through $J(h, g) = h_x g_y - h_y g_x$, and $\nu_n > 0$ is the diffusive parameter, assumed small. The non-negative integer n is the order of the diffusivity applied. The coupled equations (1) and (2) can be written as a non-linear evolution equation for ψ alone as

$$\frac{\partial}{\partial t}\left(\nabla^2\psi\right) + J\left(\psi, \nabla^2\psi\right) + \beta\frac{\partial\psi}{\partial x} = \nu_n\left(-\nabla^2\right)^{n+1}\psi. \tag{3}$$

The order of diffusivity n takes values in $\{0, 1, 2, \ldots\}$. If $n = 0$, the dissipative term corresponds to Rayleigh friction, where a frictional force proportional to the velocity is included at the momentum equation level (Gill, 1982; Wajsowicz, 1986). The most standard case $n = 1$ is 'normal' diffusivity (studied, for example, in Rhines, 1975; Balasuriya, 1997; Miller *et al.*, 1997; Rogerson *et al.*, 1999; Yuan *et al.*, 2002), or equivalently viscous dissipation. The hyper-diffusive case $n = 2$ is also used frequently in numerical modelling (Basdevant *et al.*, 1981; McWilliams, 1984; Flierl *et al.*, 1987; Babiano *et al.*, 1994; Poje *et al.*, 1999), and higher-order diffusivities such as $n = 5$ have also been studied (Marcus and Lee, 1994). The general nth-order formulation has also been used in numerical studies (Basdevant *et al.*, 1981; Macaskill and Bewick, 1995), but not in analytical ones. Equation (3) shall be considered to be in non-dimensional coordinates, in which case ν_n could be thought of as the reciprocal Péclet number associated with nth-order diffusivity. (If the length and velocities associated with such a non-dimensionalisation are L and U respectively, then ψ would be scaled by LU, ν_n by UL^{2n-1} and β by UL^{-2}.)

Though (3) is a $(2n + 2)$th-order non-linear PDE for ψ, the following is an *exact* analytical solution:

$$\psi(x, y, t) = A\exp\left[-\nu_n\left(k^2 + l^2\right)^n t\right]\sin\left[k\left(x + \frac{\beta t}{k^2 + l^2}\right)\right]\sin(ly) \tag{4}$$

for any positive wavenumbers k and l, and amplitude A. The no-slip condition of a 'true' fixed boundary cannot be satisfied by this solution, and hence its relevance in nature is to regions far removed from such boundaries. Note that this solution is valid for *all* orders of diffusivity ($n = 0, 1, 2, \ldots$), and is indeed generalisable to fractional diffusivities. While available in the literature for the standard diffusive case $n = 1$ (Balasuriya *et al.*, 1998; Balasuriya, 2001), the author is unaware of such solutions being stated for hyper-diffusivity or $n = 0$ (apart from Wajsowicz (1986), in which *linearised* dynamical equations are considered).

The non-diffusive limit is obtainable through setting $\nu_n = 0$, and then (4) becomes the standard Rossby wave solution (Pedlosky, 1979) to the barotropic, PV-conserving equation (i.e., (3) with $\nu_n = 0$). The solution (4) generalises the Rossby wave to $\nu_n \neq 0$ and to arbitrary nth-order diffusivity. In keeping with the standard Rossby wave which is an exact solution to the non-linear equation (3) with $\nu_n = 0$, this solution also possesses a fortuitous cancellation in the non-linear term $J(\psi, \nabla^2\psi)$.

Some qualitative observations are immediate from the model streamfunction (4). It incorporates an exponential damping on to the standard (non-diffusive) travelling Rossby wave. The order of diffusivity n appears only in the exponential decay. This decay rate is independent of the wavenumbers for Rayleigh friction ($n=0$). In other instances, if $k^2 + l^2 > 1$ (i.e., sufficiently small wavelengths), ψ decays more as n increases. Small scales suffer more dissipation as the order of diffusion increases. Intriguingly, if $k^2 + l^2 < 1$, increasing n *reduces* the decay rate (in particular, in the 'super-diffusive' limit $n \to \infty$, there is virtually no dissipation at these large scales!). There appears a connection with the preference for large sized coherent eddies; more on this issue is addressed in Section 6. Moreover, the difference between the streamfunction (4) and its non-diffusive counterpart is of size ν_n for finite times, in congruence with the rigorous result (Balasuriya, 1997) available for $n = 1$ for generic solutions to (3).

Though the emphasis in the remainder of this study is on the Eulerian characteristics of the solution (4), a brief paragraph on the Lagrangian implications is in order. A deterministic Eulerian velocity field (such as that corresponding to (4)) does not automatically engender regular Lagrangian particle trajectories, as has been shown in many examples (Knobloch and Weiss, 1987; Weiss and Knobloch, 1989; Pierrehumbert, 1991; Samelson, 1992; del Castillo-Negrete and Morrision, 1993; Meyers, 1994; Weiss, 1994; Pratt *et al.*, 1995). However, studies (Balasuriya *et al.*, 1998; Sandstede *et al.*, 2000; Balasuriya and Jones, 2001) suggest that some form of flow regularity exists for small ν_n when $n = 1$ (the asymptotic steadiness in a moving frame contributes to this). Nevertheless, since 'steadiness' is never in reality achieved, there is evidence (Balasuriya *et al.*, 1998; Sandstede *et al.*, 2000) that for $n = 1$ transient chaos – shift dynamics on a set of arbitrarily long symbols (Wiggins, 1988) – results.

In preparation for examining the Eulerian implications of the model, define the zonally translating variable

$$x' = x + \frac{\beta t}{k^2 + l^2}.$$

Then, the PV $q(x, y, t)$ for this solution is given by

$$q(x, y, t) = -A\left(k^2 + l^2\right)\exp\left[-\nu_n\left(k^2 + l^2\right)^n t\right]\sin(kx')\sin(ly) + f + \beta y \tag{5}$$

by applying (1). Now, in nearly PV-conserving flows, it is traditional to use PV-contours to define regions of flow behaviour. This is not to say that particles exactly follow the PV-contours, yet when the diffusivity is small, the dominant motion is along such contours. Based on this, a *Eulerian definition* of an eddy at each time t shall be a region in which the PV-contours are closed (topologically circular). Therefore, there

must exist a local extremum of the PV-field at a point within this closed contour structure.

The evolution of the contours of $q(x, y, t)$ is shown in Fig. 1. Since (5) is periodic in x, it is only necessary to sketch the contours for $-\pi/k \leq x < \pi/k$. In this figure, the values $A = 1$, $k = 1$, $l = 0.5$, $f = 0$, $\beta = 0.103$ and $\nu_n = 0.1$ are used, and the contours of q are plotted for: (a) $t = 0$; (b) $t = 5$; (c) $t = 9$ and (d) $t = 15$. Notice the presence of elliptic eddies in (a), (b) and (c), and their eventual disappearance by (d). As the contours evolve from $t = 0$ to $t = 5$, the basic structure persists, though the dissipation of PV is apparent (there are fewer contours surrounding the eddy regions in (b) than in (a)). The dissipation is more pronounced by $t = 9$ (in (c)), and indeed an asymmetry of the eddies is to be seen. Notice also a meridional drift in the eddies. By $t = 15$, the eddies have completely vanished, and an effectively shear flow structure is apparent in (d). There is apparently an intermediate time at which the eddies vanish.

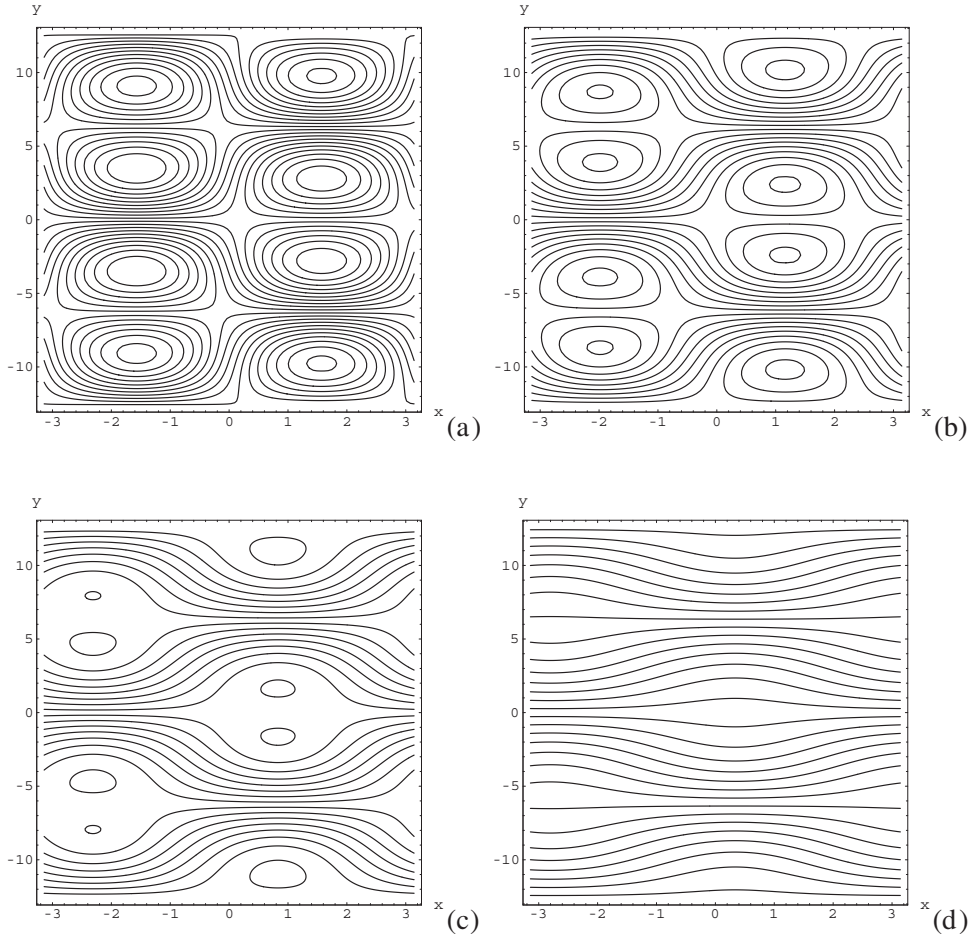

FIGURE 1 Potential vorticity contours at (a) $t = 0$, (b) $t = 5$, (c) $t = 9$ and (d) $t = 15$. The values $A = 1$, $\nu_n = 0.1$, $f = 0$, $\beta = 0.103$, $n = 2$, $k = 1$ and $l = 0.5$ are used in this figure.

A principal goal of this study is to analyse the motion, size decay and disappearance time of these vortices, and relate them to the parameters in the problem (eddy size, shape and strength, Coriolis effect, diffusivity). Now, at each time t, the eddy centres are located at local maxima or minima of the PV-field. Also important in the vortex structure are saddle points of the PV; as addressed variously in Balasuriya and Jones (2001), Haller and Poje (1997) and Weiss (1994), saddles and centres are *both* necessary for the topological structure of an eddy to be localised in a complex flow. As an example, imagine placing a vortex of initial infinite influence in a non-trivial background flow. In this case, at least one saddle point will be created, along a 'boundary' which distinguishes between regions of purely closed PV-contours, and something anomalous. See for example Figures 3–8 in Williams and Yamagata (1984), in which a Gaussian vortex is superimposed on a zonal flow, and the contours demonstrate the importance of an associated saddle point in demarcating the eddy. One might argue that the boundary saddle points reflect the interaction between the eddy and the surrounding flow; closed PV-contours are modified through adjacent effects to create such saddle points.

Both centres and saddles correspond to critical points of the PV-field, and hence it is necessary to locate points at which the PV-gradient vanishes. Using (5), we have

$$\nabla q = \begin{bmatrix} -Ak\left(k^2+l^2\right)\exp\left[-\nu_n\left(k^2+l^2\right)^n t\right]\cos kx' \sin ly \\ -Al\left(k^2+l^2\right)\exp\left[-\nu_n\left(k^2+l^2\right)^n t\right]\sin kx' \cos ly + \beta \end{bmatrix}. \tag{6}$$

Note that the parameter f does not appear in the PV-gradient. The presence (or absence) of this uniform rotation does not affect the topological structure of the PV-field, since it is a mere additive constant. In all that follows, the constant background rotation f will play no role.

At each fixed t, (6) indicates that saddles and centres are given by the solutions of

$$\cos kx' \sin ly = 0, \tag{7}$$

$$\sin kx' \cos ly = \frac{\beta}{A\,l(k^2+l^2)}\exp\left[\nu_n\left(k^2+l^2\right)^n t\right]. \tag{8}$$

As t increases, the right-hand side of (8) will eventually surpass unity, and thereafter *no* solutions would exist. Saddles and centres can be present only if

$$\frac{\beta}{Al(k^2+l^2)}\exp\left[\nu_n\left(k^2+l^2\right)^n t\right] \leq 1,$$

i.e., only if t is less than a critical lifetime T given by

$$T = \frac{1}{\nu_n(k^2+l^2)^n}\ln\frac{A\,l\left(k^2+l^2\right)}{\beta}.$$

It is shown in Section 4 that several different types of solutions to (7) and (8) exist for $t \leq T$. These solutions correspond to centres and saddles, and the motion of these Eulerian entities will be exactly quantified. It turns out that *all* these critical points

will simultaneously vanish at $t = T$, and therefore T is the lifetime of each and every one of the eddies in the flow. For reasons of notation, the analysis of eddy motion for $t < T$ will be postponed to Section 4, whereas the next section will focus on the critical lifetime.

Before the lifetime is analysed in detail, a possible viewpoint through which to examine this model is suggested. While the model which has been developed has specified values of the wavenumbers (k, l), the fact that it corresponds to an *exact* solution to (3) may render it more useful than to merely model a spatially periodic flow. Consider a flow comprising many different eddies of different length-scales, embedded in a complex background flow. Pick one eddy, and suppose that it possesses dominant wavenumbers (k, l). If so, (4) could be used as a first approximation for this eddy, in a localised region near it. In other words, (4) may be thought of as the first term in a Taylor-type expansion for the kinematical structure of the eddy, *which retains dynamical consistency* through obeying (3). As long as this eddy structure is retained, its behaviour could therefore be expected to be close to that of the elementary model (4). It should be noted that the vortice's structure is not independent of any adjacent eddies or background flow; those have dynamically conspired to create the local extremum, and attendant saddle point(s), which define this eddy (see Figures 3–8 in Williams and Yamagata (1984) to see how a Gaussian eddy is modified similarly by a shear flow).

Aberrations to this particular eddy could be caused through, for example, the effects of imposing a Rankine core in the eddy, deviations from ellipticity, interaction terms with other eddies and/or wavenumbers (this would contribute through non-linear coupling terms in (3)), baroclinicity, wind or other forcing. Given that (4) is exactly dynamically consistent, it has the potential of remaining robust to such small perturbations. The expressions that are to be derived, related to an eddy's lifetime, trajectory and size, could therefore be expected to remain grossly accurate.

3. EDDY LIFETIME ANALYSIS

It was shown that the eddies can only live until t reaches the *eddy lifetime* T given by

$$T(k, l) = \frac{1}{\nu_n (k^2 + l^2)^n} \ln \frac{A\, l \left(k^2 + l^2\right)}{\beta}. \tag{9}$$

In the $\beta = 0$ or the non-diffusive ($\nu_n = 0$) limits, this lifetime is infinity, and thus the eddy destruction process addressed here is based on a combination of the Coriolis and diffusive effects. Notice also that the lifetime is increasing with vortex strength A, consistent with common sense and also experiments (see Figure 11 in Stegner and Zeitlin (1998)). The wavenumbers (k, l) include information on the eccentricity and size of the eddy; hence (9) provides information on which types of eddies persist longer.

It helps to represent (9) with respect to polar coordinates (K, η) in (k, l) space. Since $k, l > 0$, the condition $0 < \eta < \pi/2$ applies. Then

$$T(K, \eta) = \frac{1}{\nu_n K^{2n}} \ln \frac{A\, K^3 \sin \eta}{\beta}. \tag{10}$$

In the Rayleigh friction case $n = 0$, the lifetime is proportional to $\ln K$, and therefore will not have a well-defined maximum. The fact that smaller eddies live longer is counter-intuitive, and is a reflection of the fact that for Rayleigh friction, the 'diffusive' time-scale in (4) is independent of the length-scale. The remainder of this section examines $n \geq 1$ diffusivity, in which the lifetime has a non-monotonic variation with the wavenumber magnitude K.

The non-negative contours of the lifetime T in wavenumber space are shown as solid curves in Fig. 2, for the choice of constants $A = 1$, $\nu_n = 0.1$, $\beta = 0.103$ and $n = 2$. The global maximum of T is located at around $(k, l) = (0, 0.75)$, and there is a sharp gradient associated with the region where T passes through 0. In fact, this is an important transition, since if the eddy is to exist at time zero, one needs $T \geq 0$. This is fulfilled if

$$K \geq \left(\frac{\beta}{A \sin \eta}\right)^{1/3}. \tag{11}$$

The parameters chosen in Fig. 1 conform to this. Notice that the Coriolis effect β and the eddy strength parameter A compete in determining allowable wavenumbers. The region corresponding to this condition in (k, l) wavenumber space is illustrated in Fig. 3. The three different curves which asymptote to the k axis correspond to different values of β/A; from the uppermost to the lowermost, these correspond to $\beta/A = 2$, 1 and 0.103, respectively. In each case, the condition (11) consists of

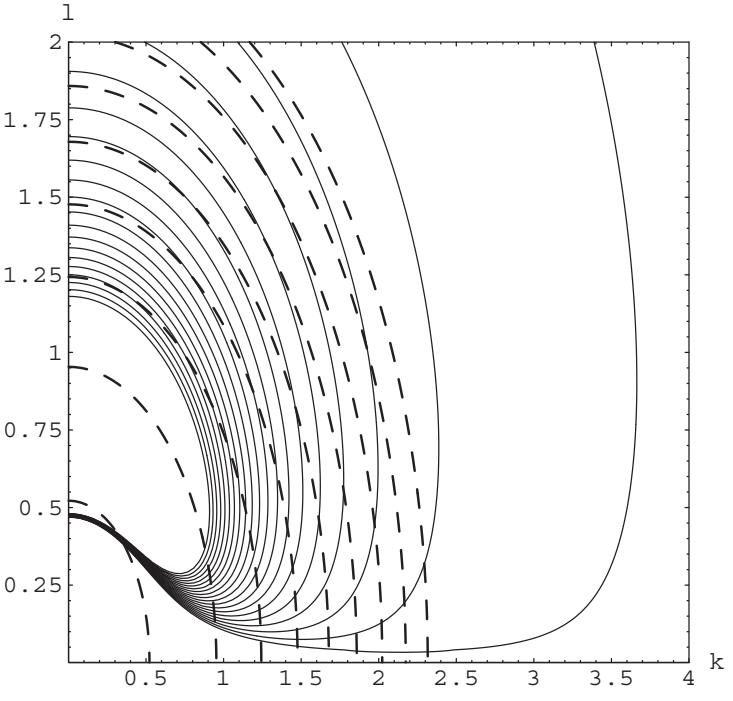

FIGURE 2 Contours of $T(k, l)$ (solid curves) in wavenumber space, with $A = 1$, $\nu_n = 0.1$, $\beta = 0.103$ and $n = 2$. The dashed curves are contours of $K = \sqrt{k^2 + l^2}$.

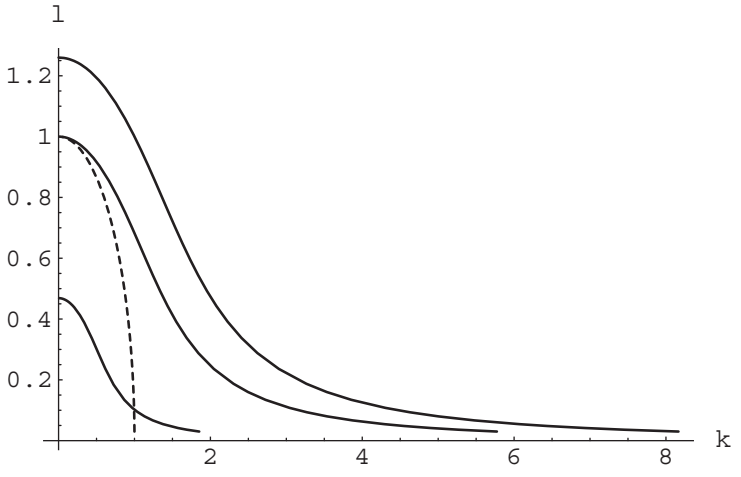

FIGURE 3 Allowable wavenumbers for different values of β/A: from uppermost to lowermost curves, $\beta/A = 2$, 1 and 0.103. The region above each curve is allowable. The dashed line is the curve $K = 1$.

the region *above* the curve. As β increases, fewer wavenumbers become available. This can be interpreted as the flow becoming more ordered for large β, consistent with observations (Rhines, 1975). On the other hand, *any* value of K is possible if A is sufficiently large. Since A represents the strength of the vortex, if the initial vortex is 'too large' but has sufficient energy, it can survive despite the Coriolis effect. The competition between β and A has been recognised in many other studies. For example, Llewellyn Smith (1997) and Reznik and Dewar (1994) effectively use β/A as a perturbation parameter in obtaining asymptotic axisymmetric eddy solutions.

Also illustrated in Fig. 3 is the dashed unit circle $K = 1$ in wavenumber space. If larger eddies are to be seen, it is clear from the figure that one needs β sufficiently small. For example, the only eddies of size $K < 1$ that can be present in a geophysical flow with $\beta/A = 0.103$, must have wavenumbers below the dashed curve but above the $\beta/A = 0.103$ curve of Fig. 3. Thus, the competition between planetary and nonlinear effects produces a length-scale parameter, which has been argued to separate the quasi-geostrophic, intermediate-geostrophic and planetary-geostrophic scales (Williams and Yamagata, 1984).

The elliptic eddies described here could be defined to have an anisotropy (or eccentricity) parameter obtained by dividing their y-extent by their x-extent. This takes the value $k/l = \cot\eta$, and therefore η represents the eccentricity of the eddy. A circular (axisymmetric, isotropic) eddy, for example, has $\eta = \pi/4$. For a fixed eccentricity η, the longest-lived eddy's K value can be determined by

$$\frac{\partial T}{\partial K} = \frac{1}{\nu_n K^{2n+1}}\left(3 - 2n\ln\frac{A\,K^3\sin\eta}{\beta}\right),$$

which is zero (and corresponds to a maximum of T) when

$$K = K_m := e^{1/(2n)}\left(\frac{\beta}{A\sin\eta}\right)^{1/3}. \tag{12}$$

The longest-lived eddies are larger as one proceeds away from the equator; a result consistent with atmospheric observations that in higher latitudes, energy spectra are predominantly in the low wavenumber region (Kao and Wendell, 1970). Moreover, the longest lived eddy is larger under higher-order diffusivities.

The maximum lifetime corresponding to the longest-lived eddy of fixed eccentricity is

$$T(K_m, \eta) = \frac{3}{2en\nu_n}\left(\frac{A\sin\eta}{\beta}\right)^{2n/3}. \tag{13}$$

This again has many implications (for example, this lifetime depends on the Coriolis parameter in the form $\beta^{-2n/3}$). As β decreases (as one proceeds further from the equator), this maximum lifetime increases. Thus coherence (both in terms of size and lifetime) of eddies improves further away from the equator.

Define an eddy's length-scale by $L = 1/K$. One may represent T as a function of L as

$$T(L) = \frac{L^{2n}}{\nu_n}\ln\frac{A\sin\eta}{\beta L^3}.$$

A plot of T as a function of the eddy length-scale L is shown in Fig. 4. The values $A = 1$, $\nu_n = 0.1$, $\beta = 0.103$, $\eta = \pi/4$ and $n = 2$ have been used in this figure. The length-scale corresponding to the maximum lifetime is, from (12),

$$L_m = \frac{1}{K_m} = e^{-1/(2n)}\left(\frac{A\sin\eta}{\beta}\right)^{1/3}.$$

The observation by Rhines (1975) that increasing β decreases the spatial scale (see his Figure 6) is borne out by this equation. Indeed, since $T \geq 0$ is required,

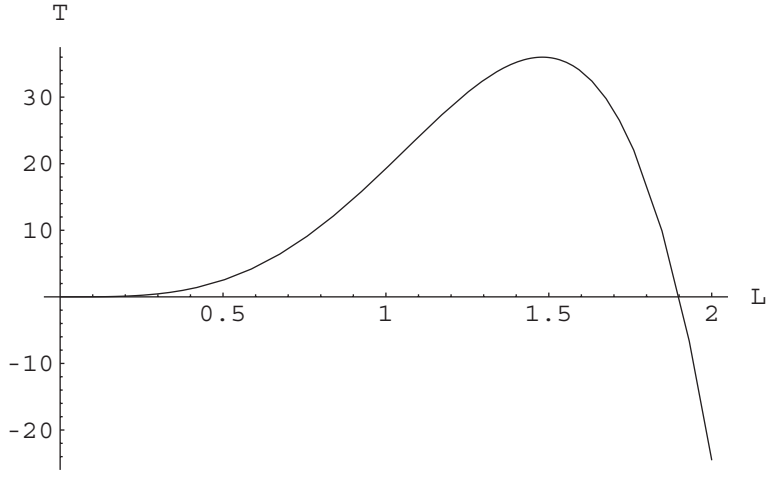

FIGURE 4 Lifetime *versus* length-scale: $A = 1$, $\nu_n = 0.1$, $\beta = 0.103$, $\eta = \pi/4$ and $n = 2$.

$L \leq (A \sin \eta/\beta)^{1/3}$ gives the range of permitted sizes of eddies. Moreover, T decreases to zero as $L \to 0$; the smaller the eddy, the quicker it disappears.

As η reduces, the eddy's lifetime diminishes. That is, an elliptic eddy with a larger meridional extent (in comparison with its zonal extent), has virtually no chance of survival. Eddies with the reverse geometry, on the other hand, are longer-lived.

Figure 2 also provides intuition into atmospheric observations that, for small wavenumbers, energy resides mainly in the zonal velocities, whereas for high wavenumbers, zonal and meridional modes have approximately the same energy (Eliasen, 1958; Kenyon, 1967; Kao and Wendell, 1970; Baer, 1972). The dashed lines show $K =$ constant contours in the wavenumber space. Observe that for smaller values of K, travelling along such a contour in the direction of increasing η would mean that the lifetime contours are being sharply intersected, and thereby the lifetime is increasing. In contrast, the K-contours for larger values of K tend to align better with the T-contours; the lifetime is increasing much more slowly. It is reasonable to expect observed eddies to be the ones which have a larger lifetime; hence for small K, larger values of η are to be expected, in contrast to large K, where changing η has much less effect on the lifetime.

Figure 5 explores this in greater detail. The variation of the lifetime with η is presented for three different K values. As K increases the curves move towards the left, enabling more η values to become admissible. The larger vortices corresponding to $K = 0.6$ are about fifty times longer-lived than the smaller $K = 2.0$ vortices. Moreover, as K increases, the curves become less steep, and indeed by $K = 2.0$, have become so flat that there appears hardly any bias towards any of the permitted values of η. In a flow containing only large wavenumbers K, since no particular η is favoured to persist longer, a large spectrum of η values would be observed. On the other hand, if a flow contained only small wavenumbers K, vortices corresponding to an anisotropy in which k is small but l is large (i.e., eddies with a larger zonal extent) should be seen more. Since an energy computation at some given time would be more likely to capture the longer-lived vortices, this model gives a plausible view on the observed dichotomy between small and large wavenumbers in the atmosphere.

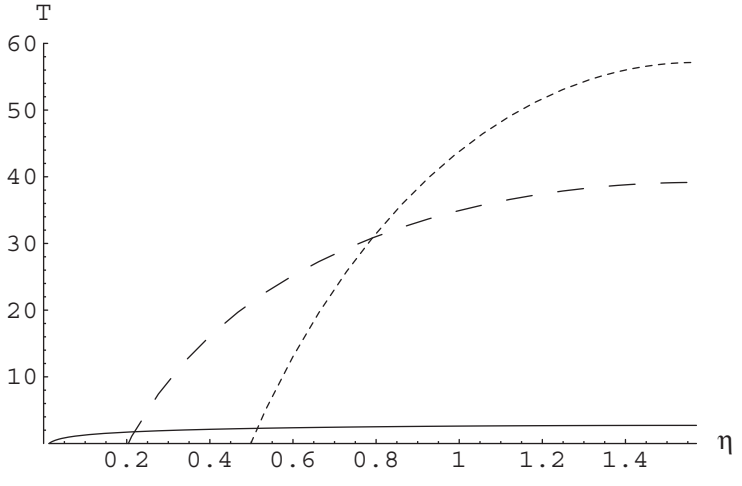

FIGURE 5 Variation of $T(K, \eta)$ with η for fixed K: $K = 0.6$ (short dashes), $K = 0.8$ (long dashes) and $K = 2.0$ (solid). In all cases, $A = 1$, $\nu_n = 0.1$, $\beta = 0.103$ and $n = 2$.

4. EDDY MOTION

This section returns to the motion of the vortices, until the time of their disappearance. To examine more closely the eddy behaviour in Fig. 1, a large-scale portrait is presented in Fig. 6. This pertains to exactly the same parameter values as Fig. 1, while focusing on a smaller region adjacent to a pair of eddies. The times at which the contours are displayed are (a) $t = 10$, (b) $t = 11.2$ and (c) $t = 11.7$. In Fig. 6(a), there are two adjacent eddies (the upper one stronger, and of opposite sign, than the lower), characterised as usual by closed PV-contours. There are local extrema (centres) within these contours. There are also two saddle points, around the locations $(-3.1, -6.5)$ and $(-1.7, -6.5)$, which one can assume from this picture. As time proceeds to $t = 11.2$, the eddies have shrunk in size (there are in fact still two eddies present, though the lower one is much weaker than the upper, and hence is not visible in Fig. 6(b)). Notice that the upper centre has moved southwards, and an extrapolation of the visible contours suggests that the lower centre has moved northwards. Therefore, in addition to westward motion at the Rossby wave speed, a meridional drift is present.

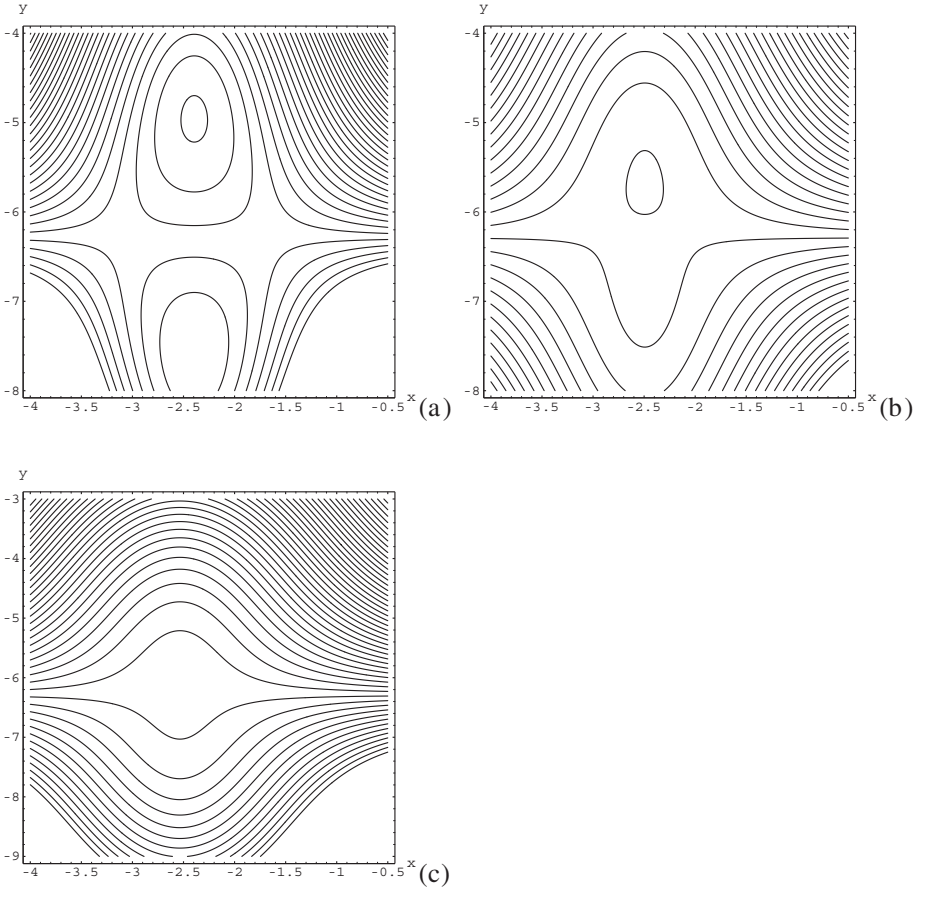

FIGURE 6 A closer look at eddy disappearance: (a) $t = 10$, (b) $t = 11.2$ and (c) $t = 11.7$. The values $A = 1$, $\nu_n = 0.1$, $f = 0$, $\beta = 0.103$, $n = 2$, $k = 1$ and $l = 0.5$ are used in this figure.

By $t = 11.7$, in Fig. 6(c), the centres and saddles have both disappeared, and as a consequence, there are no more Eulerian eddies in the flow.

To analyse this behaviour, return to the analytical expressions of Section 2. For $t \le T$, the Eqs. (7) and (8), corresponding to points of vanishing PV-gradient, have two types of solutions. One corresponds to the first term in (7) being zero, and the other to the second term vanishing. Given q's periodicity in x, in determining these solutions, attention will be restricted to $-\pi/k \le x < \pi/k$. Indeed, one may identify the line $x = -\pi/k$ with $x = \pi/k$, and thus effectively examine motion on a cylinder. The nature of the critical points is governed by the sign of the Hessian $H = q_{xx}q_{yy} - (q_{xy})^2$, which has a general value

$$H = A^2K^8 \cos\eta \sin\eta \exp\left(-2\nu_n K^{2n} t\right)\left(\sin^2 kx' \sin^2 ly - \cos^2 kx' \cos^2 ly\right),$$

where (K, η) are the polar coordinates of the wavenumbers (k, l) as outlined in Section 3.

If $\sin ly = 0$, then $y = p\pi/l$, where p is any integer. Then from (8), we have

$$\sin kx' = \frac{(-1)^p \beta \exp\left[\nu_n\left(k^2 + l^2\right)^n t\right]}{Al(k^2 + l^2)}.$$

If p is even, the solutions x' are positive and symmetric about $\pi/(2k)$, whereas for odd p, they are negative and symmetric about $-\pi/(2k)$. We define

$$\gamma(t) \equiv \cos^{-1}\left\{\frac{\beta \exp\left[\nu_n\left(k^2 + l^2\right)^n t\right]}{Al(k^2 + l^2)}\right\} = \cos^{-1}\left[\frac{\beta \exp\left(\nu_n K^{2n} t\right)}{AK^3 \sin\eta}\right], \tag{14}$$

where $0 \le \gamma(t) < \pi/2$. Notice that γ is monotonically decreasing with time t, and that $\gamma \to 0$ as $t \to T$. Then, the even and odd p solutions are given respectively by

$$x' = \frac{\pi}{2k} \pm \frac{\gamma(t)}{k} \quad \text{and} \quad x' = -\frac{\pi}{2k} \pm \frac{\gamma(t)}{k}.$$

Since $\sin ly = 0$ at these points, H is clearly negative, and therefore all these points are saddle points of q. These saddle points have a fixed y coordinate, but x' changes with time.

The second case one needs to consider from (7) is when $\cos kx' = 0$. This corresponds to $x' = \pm\pi/(2k)$. The positivity of the Hessian implies these are eddy centres. Equation (8) then gives $\cos ly = \pm\cos\gamma(t)$, from which

$$y = \frac{2p\pi}{l} \pm \frac{\gamma(t)}{l} \quad \text{or} \quad y = \frac{(2p+1)\pi}{l} \pm \frac{\gamma(t)}{l}$$

are the solutions for the positive and negative sign choices respectively, for any integer p. The next step is to determine the directions of rotations of these eddies. Since the β-plane approximation is best used close to $y = 0$, this shall be done only for the eddies near this meridion. Choosing $p = 0$ in each of the above expressions gives four such eddies, one in each of the quadrants in (x', y) space. Now, the motion of

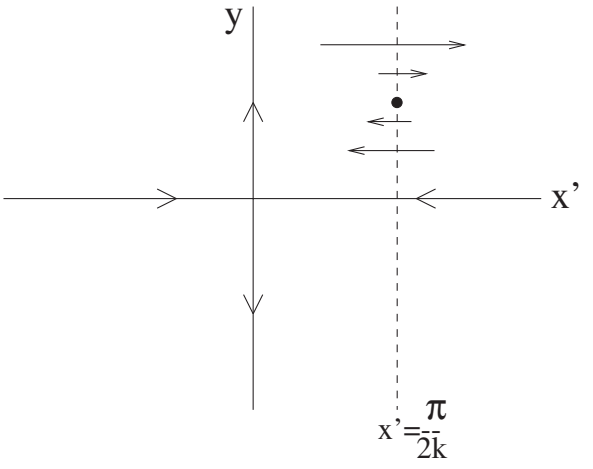

FIGURE 7 Particle trajectory directions based on (15), which are used to determine the direction of rotation of the eddy in the first quadrant.

particles is governed by

$$\begin{aligned} \dot{x} &= -\psi_y = -Al \exp\left[-\nu_n\left(k^2+l^2\right)^n t\right] \sin kx' \cos ly, \\ \dot{y} &= \psi_x = Ak \exp\left[-\nu_n\left(k^2+l^2\right)^n t\right] \cos kx' \sin ly. \end{aligned} \tag{15}$$

The directions of motion along the $x' = 0$, $x' = \pi/(2k)$ and $y = 0$ axes are displayed in Fig. 7. The eddy located in the first quadrant thus clearly has a clockwise rotation, at a given instance in time t.

Performing this analysis on the centres C and saddles S near the meridion $y = 0$ enables the exact positions of these entities in (x, y) space to be determined:

$$\begin{aligned} S_1: &\quad \left(-\frac{\beta t}{(k^2+l^2)} + \frac{\pi}{2k} - \frac{\gamma(t)}{k}, 0\right), \\ S_2: &\quad \left(-\frac{\beta t}{(k^2+l^2)} + \frac{\pi}{2k} + \frac{\gamma(t)}{k}, 0\right), \\ S_3: &\quad \left(-\frac{\beta t}{(k^2+l^2)} - \frac{\pi}{2k} - \frac{\gamma(t)}{k}, \frac{\pi}{l}\right), \\ S_4: &\quad \left(-\frac{\beta t}{(k^2+l^2)} - \frac{\pi}{2k} + \frac{\gamma(t)}{k}, \frac{\pi}{l}\right), \\ C_1: &\quad \left(-\frac{\beta t}{(k^2+l^2)} + \frac{\pi}{2k}, \frac{\gamma(t)}{l}\right), \\ C_2: &\quad \left(-\frac{\beta t}{(k^2+l^2)} - \frac{\pi}{2k}, \frac{\pi}{l} - \frac{\gamma(t)}{l}\right), \\ C_3: &\quad \left(-\frac{\beta t}{(k^2+l^2)} - \frac{\pi}{2k}, -\frac{\pi}{l} + \frac{\gamma(t)}{l}\right), \\ C_4: &\quad \left(-\frac{\beta t}{(k^2+l^2)} + \frac{\pi}{2k}, -\frac{\gamma(t)}{l}\right). \end{aligned}$$

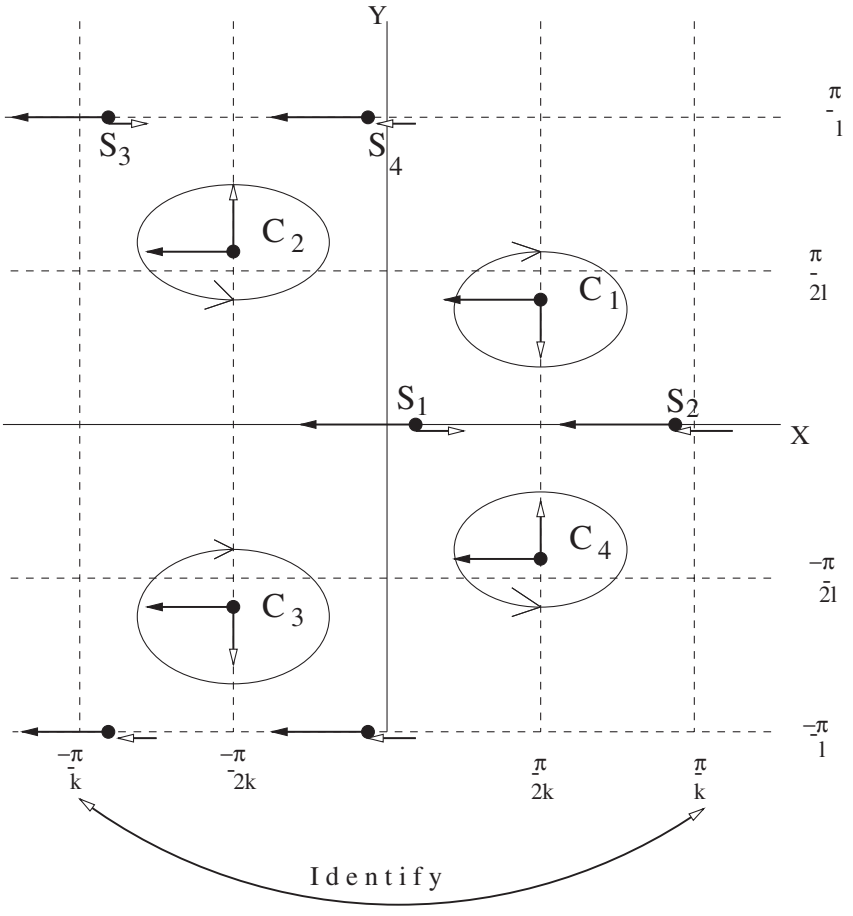

FIGURE 8 Schematic of the motion of eddy centres and saddles near $y = 0$. The solid arrows give the easterly Rossby wave drift, and the open arrows are the additional velocities as described in the text.

These centres and saddles are displayed in Fig. 8, with the rotational directions of the centres also specified. This sketch is in the (x, y) frame, and in converting from x' to x, it must be noted that *all* entities must translate westward at the Rossby wave speed $\beta/(k^2 + l^2)$. These motions are indicated in the figure with arrows with solid heads. The additional motion caused through the presence of $\gamma(t)$ is indicated with arrows with open heads. The velocity directions are determined by using the derivatives of the above positions, and bearing in mind that $\dot{\gamma}(t) < 0$.

The saddle S_2 is travelling westward faster than S_1, and will eventually catch up with it. Meanwhile, the eddy centres C_1 and C_4 are approaching the meridion $y = 0$. Indeed, if one examines the limit $t \to T$ for *all* of these four entities, they approach the identical location

$$\left(-\frac{\beta T}{(k^2 + l^2)} + \frac{\pi}{2k}, 0\right).$$

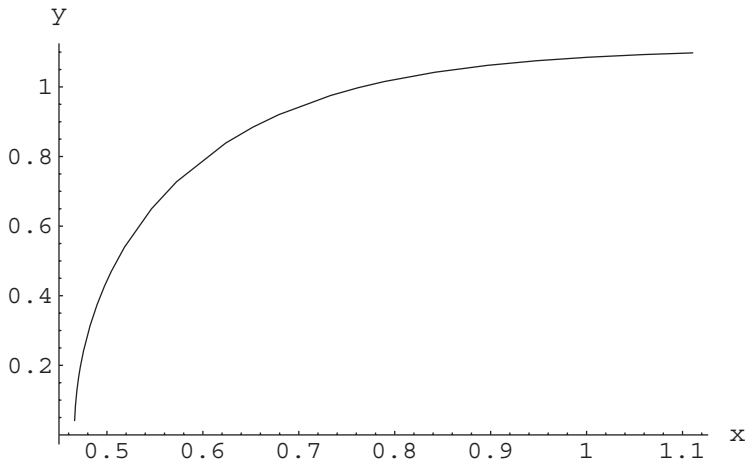

FIGURE 9 The trajectory of the vortex C_1 as time progresses (it is travelling in the southwest direction). The values $v_n = 0.01$, $A = 1$, $\eta = \pi/4$, $K = 2$, $\beta = 0.103$ and $n = 2$ have been used.

Two saddles and two eddy centres simultaneously coalesce and disappear at this location at $t = T$. This same sort of behaviour occurs in the disappearance of the other eddies and saddles, as the lifetime (9) is approached. The eddies of this model therefore are dipoles, whose counter-rotating parts fuse upon reading the eddy lifetime.

The exact trajectories of the eddy centre C_1 in (x, y) space are shown in Fig. 9 for the choice of parameters $v_n = 0.01$, $A = 1$, $\eta = \pi/4$, $r = 2$, $\beta = 0.103$ and $n = 2$. Beginning at a certain meridional value, the eddy initially moves mainly westward, but the meridional drift amplifies as time progresses, and the eddy approaches $y = 0$ tangential to the northward direction. This qualitative form of barotropic vortex motion has been presented in many other analytical and numerical studies; see Figure 1 in Reznik (1992), Figure 4 in Sutyrin *et al.* (1994), or the curve labelled "model" in Figure 1 in Reznik and Dewar (1994). There are other studies which show somewhat different vortex trajectories: Llewellyn Smith (1997)'s Figure 2, and Carnevale *et al.* (1991)'s Figure 2, appear to have the opposite behaviour of levelling out as time progresses, and linear trajectories result from other approximations (Smith and Ulrich, 1990; Korotaev and Fedotov, 1994; Reznik and Dewar, 1994).

The fact that cyclonic eddies drift polewards, and anti-cyclonic ones towards the equator, can be obtained from this model. If in the northern hemisphere, the anti-clockwise vortices C_2 and C_4 of Fig. 8 are cyclonic, and C_1 and C_3 are anti-cyclonic. The cyclonic vortices, through the effect produced through $\gamma(t)$, move poleward, whereas the anti-cyclonic ones move towards the equator. On the other hand, if in the southern hemisphere, the vortices have the reverse cyclonicity. Nevertheless, the rule for poleward drift for cyclonic vortices is seen to be still valid. This is true for *all* vortices (pictured in Fig. 8 or not) emerging from this model. It is moreover possible to exactly characterise the speed of meridional drift, which is the same for *all* vortices of this model:

$$\left|\dot{y}(t)\right| = -\frac{\dot{\gamma}(t)}{l} = \frac{\beta v_n K^{2n-1}}{\sin\eta\sqrt{A^2K^6\sin^2\eta\exp(-2v_nK^{2n}t) - \beta^2}}. \tag{16}$$

It should be noted that this is *not* the standard meridional Rossby wavespeed (which would be $\beta \cot \eta / K^2$), but rather the meridional speed of the PV-centres. The monotonic increase with t of the meridional speed has been seen in other studies (McWilliams and Flierl, 1979; Reznik, 1992; Reznik and Dewar, 1994; Sutyrin *et al.*, 1994). The speed moreover becomes infinite at precisely the vortex lifetime (9), and so this singularity is associated with the disappearance of the vortex. Within the times of existence, (16) is also an increasing function of the parameter β/A. Strong eddies (large A in comparison to β) resist meridional drift. This idea works well with the experiments of Stegner and Zeitlin (1998), who in their Figure 12 essentially show this effect. They use a larger volume of injection to create stronger vortices, and hence this paper's A is related to their abscissa in Figure 12.

Eddies which are created with a large meridional extent ($\eta \approx 0$) will translate very rapidly in the meridional direction, but have a very short life expectancy, as described in Section 3. Also notice that smaller magnitudes of diffusivity cause lesser drift (indeed, if $\nu_n = 0$, (4) is a simple travelling Rossby wave with *only* zonal motion). Hyper-diffusion is therefore a mechanism in this model which contributes towards drift. While many other studies exhibiting meridional drift are based on non-diffusive models (Rossby, 1948; Adem, 1956; Korotaev and Fedotov, 1994; Reznik, 1992; Reznik and Dewar, 1994; Llewellyn Smith, 1997; Sutyrin *et al.*, 1994; Smith and Ulrich, 1990), the present phenomenon presumably adds to the nonlinear drift effects discussed therein. Numerical diffusivity may also play a role in the numerical studies.

The variation of the drift speed (16) with respect to vortex size is less obvious, and apparently has a strong dependence on the order of diffusivity n. Plotting this dependence for different values of n needs care, since the scale in (16) changes substantially for different n, and also since the conditions (11) and $t \leq T$ must both be satisfied for the parameters chosen. Examining (16), one would expect the speed to increase with K for large enough n, and decrease with K for small n. Figure 10 demonstrates this behaviour. Each panel shows the variation of the speed with the reciprocal length-scale K, for a fixed value of n. Since higher values of n ($n = 3, 4, \ldots$) turn out to have qualitatively similar behaviour to $n = 2$, some fractional values of n are also included in this figure (such n would represent fractional-order Laplacian derivatives in the dynamical equation (3); the model solution is generalisable to such values). In any case, the observation is that higher orders of diffusivity typically translate *smaller* vortices faster, whereas lower orders of diffusivity are more effective in causing meridional motion of larger vortices.

The meridional motion vanishes in the limit $\beta = 0$, which is the uniform background rotational limit since f in (1) may be non-zero. Since $\gamma(t)$ is identically zero, saddles and centres simply translate westwards at the classical Rossby wave speed. No eddy disappearance occurs. Indeed, the solution (4) is then an exponentially damped stationary wave.

5. DECAY IN VORTEX SIZE

While the dependence of an eddy's lifetime on the parameters in the problem has been analysed in Section 3, the rate of the eddy's diffusive decay during its lifetime was not presented. The arguments of Section 4 enable a quick investigation of this.

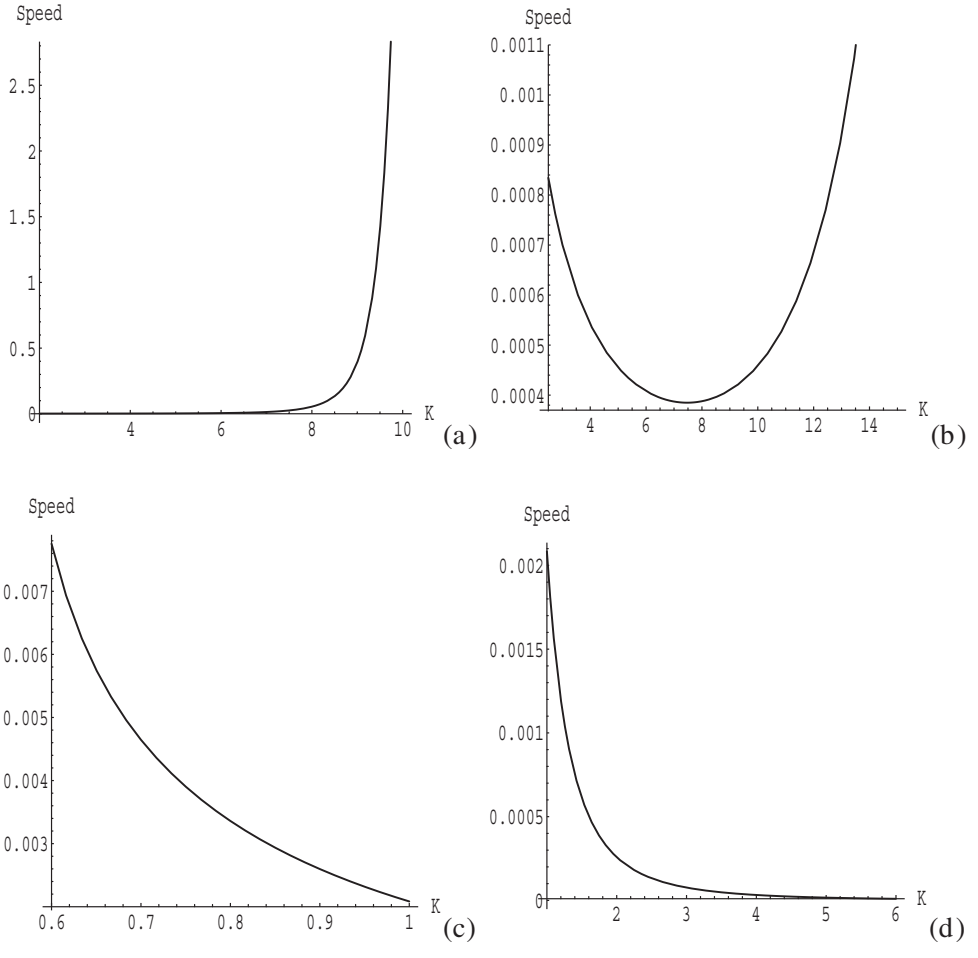

FIGURE 10 The variation of the meridional drift speed at fixed time with reciprocal length-scale K. The other parameters chosen are $A = 1$, $\nu_n = 0.01$, $\eta = \pi/4$ and $t = 0.08$. The panels correspond to different orders of diffusivity: (a) $n = 2$, (b) $n = 1.5$, (c) $n = 1$ and (d) $n = 0.5$.

During its lifetime, an eddy's size diminishes in the sense that the distance between the eddy centre and one of the associated saddle points decreases to zero. For the eddy C_1, if choosing S_1 as the saddle point towards which C_1 converges, the relevant distance at a general time t is

$$s(t) = \sqrt{\left(\frac{\gamma(t)}{k}\right)^2 + \left(\frac{\gamma(t)}{l}\right)^2} = \frac{2\gamma(t)}{K \sin 2\eta}, \tag{17}$$

where $\gamma(t)$ is defined in (14). As $t \to T$, $s(t) \to 0$. Since the eddy disappears through a coalition between the centre (enclosed by closed PV-contours) and the saddle (reflecting external effects), the above expression demonstrates how the competition between the vortex and its surroundings unfolds.

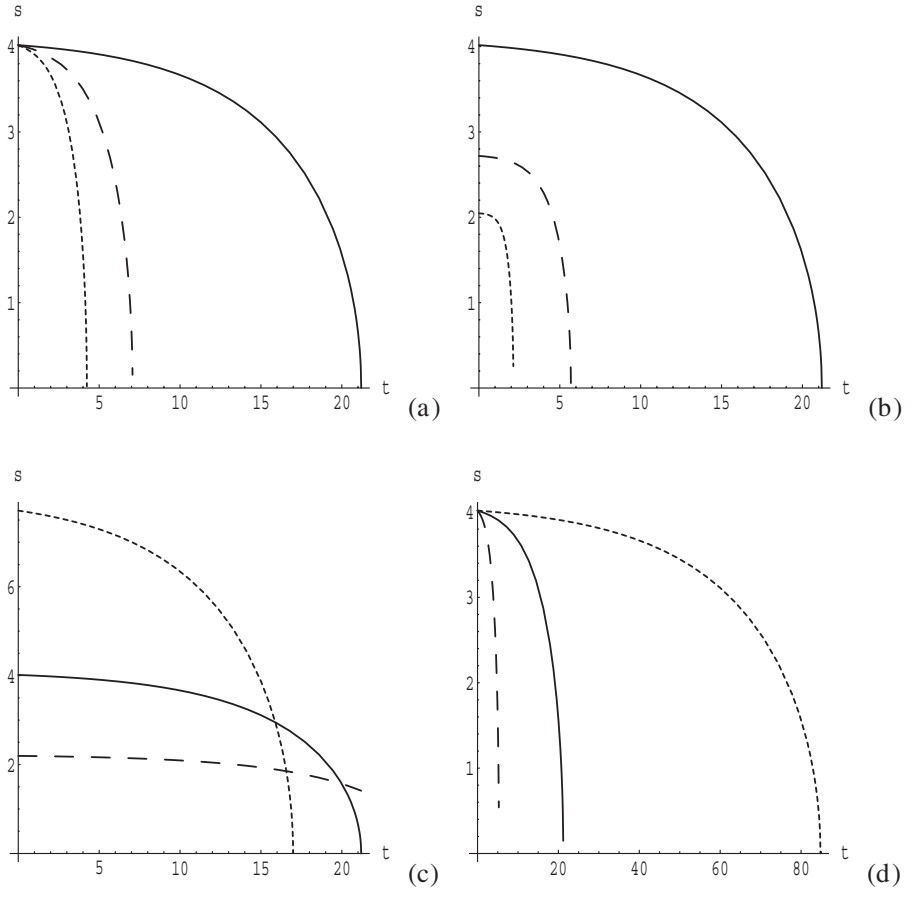

FIGURE 11 The size variation $s(t)$ of an eddy with time. The 'base' parameter values, corresponding to the solid curves in each panel, are $\beta = 0.103$, $A = 1$, $K = 2$, $\eta = \pi/8$, $n = 2$ and $\nu_n = 0.01$. (a) $\nu_n = 0.05$ (dotted) and $\nu_n = 0.03$ (dashed); (b) $K = 4$ (dotted) and $K = 3$ (dashed); (c) $\eta = \pi/16$ (dotted) and $\eta = \pi/4$ (dashed); (d) $n = 1$ (dotted) and $n = 3$ (dashed).

The distance between the eddy centre and a saddle point (which lies on the eddy boundary) is a plausible expression to use as a measure of the size of an eddy. This is particularly valuable since its variation with time is explicitly available in (17). The size variation $s(t)$ depends on the various parameters in a non-trivial way, as is illustrated in Fig. 11. In all panels, the solid curves correspond to the parameter values $\beta = 0.103$, $A = 1$, $K = 2$, $\eta = \pi/8$, $n = 2$ and $\nu_n = 0.01$. All eddies have a comparatively slow decay initially, with rapid size depreciation towards the end of their lifetime. Indeed, the curves in Fig. 11 show that half of an eddy's size is lost during roughly the final 8% of its life. Figure 11(a) displays the result of varying ν_n; the dotted curve is $\nu_n = 0.05$ and the dashed curve $\nu_n = 0.03$, with all other parameters fixed at the base values. Larger Péclet numbers cause the eddy to decay slower.

The effect of varying the initial reciprocal length-scale K is shown in Fig. 11(b), where $K = 4$ is the dotted curve, $K = 3$ the dashed, and $K = 2$ the solid. Figure 11(c) illustrates the effect of varying the eccentricity η: the dotted and dashed curves are $\eta = \pi/16$ and $\pi/4$, respectively. The monotonic effect of η on the lifetime T (as reflected

in (10) and also as the intersection coordinate of the abscissa in Fig. 11), is apparent. The dashed curve corresponding to small η decays before the others, in spite of a considerable initial advantage in size. The final panel, Fig 11(d), demonstrates the eddy's size variation dependence on the order of diffusivity n. Here, the solid curve is $n = 2$, the dotted standard diffusivity ($n = 1$), and the dashed a higher-order hyper-diffusivity ($n = 3$). Observe that lower-order diffusivity causes a much flatter decay curve (and, as known from Section 3, a much larger lifetime).

The influence of β and A on $s(t)$ has not been pictured in Fig. 11. Their effect is straightforward, since $\gamma(t)$ varies monotonically with the ratio β/A. Increasing this ratio makes $s(t)$ smaller at any value of t. Therefore, a larger Coriolis effect, or equivalently a weaker vortex, will cause quicker reduction in vortex size. While none of the results of this section are surprising, it is nonetheless useful to possess a model (17) which characterises the size variation in a hyper-diffusively decaying eddy.

6. ENERGETICS

The energy associated with the vortices can be assessed directly. Given ψ's periodicity in both x and y, it suffices to compute the kinetic energy within the unit cell $[-\pi/k, \pi/k] \times [-\pi/l, \pi/l]$, which is

$$E = \int_{-\pi/l}^{\pi/l} \int_{-\pi/k}^{\pi/k} \tfrac{1}{2} \left|\nabla\psi\right| \mathrm{d}x\, \mathrm{d}y.$$

Upon evaluation for ψ as given in (4), this yields

$$E(L, t, \eta) = \frac{\pi^2 A^2}{\sin 2\eta} \exp\left(-\frac{2\nu_n t}{L^{2n}}\right), \tag{18}$$

where the length-scale L is as defined in Section 3. The minimum E achieves with respect to η is when $\eta = \pi/4$; this model quickly gives the result that exactly circular (i.e., axisymmetric) vortices correspond to a minimum energy configuration. Thus, they are stable in the sense of variations in η. Experiments have confirmed this (McWilliams, 1984; McWilliams, 1990; Hopfinger and van Heijst, 1993). Thus, though large values of η apparently correspond to longer lifetimes where diffusivity and Coriolis effect are concerned (see Section 3), they are less stable towards fluctuations than axisymmetric vortices.

The energy density (energy per unit area), $e(L, t)$, is obtained by dividing (18) by the area of the unit cell, resulting in

$$e(L, t) = \frac{A^2}{8L^2} \exp\left(-\frac{2\nu_n t}{L^{2n}}\right). \tag{19}$$

Large vortices have a *smaller* decay rate constant (except for Rayleigh friction, where both E and e have decay constants independent of the length-scale). For small vortices ($L < 1$), the energy decay rate increases with increasing n. On the other hand, for large

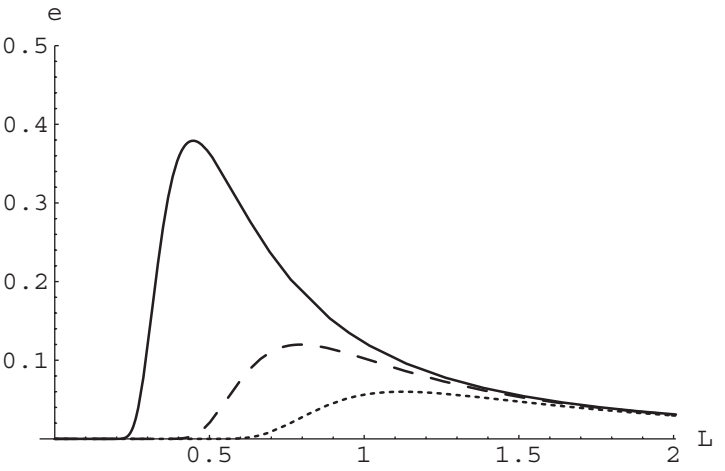

FIGURE 12 Energy density *versus* length-scale at different values of t: $t = 0.1$ (solid line), $t = 1$ (dashed line), and $t = 4$ (dotted line). Here, $A = 1$, $\nu_n = 0.1$ and $n = 2$.

vortices ($L > 1$), the decay rate is *smaller* for higher-order diffusivity. A transition in the dependence on n occurs at $L = 1$, which is the length-scale associated with the non-dimensionalising used to arrive at (3) (e.g., $L = 1$ may correspond to the Rossby deformation radius (Pedlosky, 1979), or the Rhines critical meanders scale (Rhines, 1975; Cushman-Roisin, 1994)). The observed minimum size of persistent coherent vortices may be related to this transitional length-scale.

The behaviour of the energy density (19) as a function of the length-scale is shown in Fig. 12 for different values of time. As time progresses the curve shifts down (energy dissipates), but also shifts to the right. At each time there is a preferred length-scale which maximises the energy density:

$$L = \bar{L} \equiv (2\nu_n n t)^{1/(2n)}. \tag{20}$$

This shifts to the right as t increases, and indeed the root dependence in time is qualitatively consistent with that obtained by Rhines (1975) using a heuristic argument in his Figure 1. The value of $\bar{L}$ may represent the preferred size of coherent vortices which are seen to emerge (Hopfinger and van Heijst, 1993; McWilliams, 1984; Williams and Yamagata, 1984; van Heijst and Clercx, 1998); coherent eddies are, after all, monochromatic to a gross approximation at this stage. Since $\bar{L}$ increases with time, eddies may attempt to remain energetically favourable by also increasing their size appropriately. If so, notice that the corresponding energy density

$$e(\bar{L}, t) = \frac{A^2}{8(2e\nu_n n t)^{1/n}}$$

dissipates with time, whereas the total energy within the eddy

$$E(\bar{L}, t) = \frac{\pi^2 A^2}{e^{1/n} \sin 2\eta}$$

remains constant. While the coherent eddy gains energy through absorption of adjacent areas to compensate for its diffusive dissipation, its energy density decreases because of the addition of less energetic regions.

In the limit $n \to \infty$ (arbitrarily high-order diffusivity), L'Hopital's Rule can be used on (20) to show that $\bar{L}$ approaches the limit 1, and the cascade stops. In dimensional coordinates, this would be the scaling length-scale used to obtain the dynamical equation (3). Notice moreover that this is independent of time and the diffusivity parameter ν_n. Under such 'super-diffusivity' an exactly preferred persistent length-scale for coherent eddies, equivalent to the scaling length-scale, therefore emerges. Interestingly, this is quite consistent with thinking of the Rhines scale as a scale at which the energy cascade is suppressed (Rhines, 1975).

7. CONCLUSIONS

This article has used a nontraditional viewpoint in examining barotropic vortex motion, lifetime and structure. The model was based on a generalised Rossby wave solution to the dynamical equation with general nth-order diffusivity. For non-zero β and ν_n, barotropic eddies were shown to translate exhibiting meridional drift, and then disappear at a specified time, for which an explicit expression was obtained. An exact formulation for the eddy's trajectory, and meridional drift speed (which moreover conformed with the poleward drift of cyclonic vortices), was obtained. Only eddies of certain geometries were permitted to exist under these dynamics. Micro-eddies survive only briefly. It was also seen that larger and longer-lived vortices were more likely further away from the equator. Sufficiently large eddies were also shown to have increased robustness under higher-order diffusivity. Zonal lengthening is favoured in large eddies, in contrast to small eddies, which are more isotropic. Energetically however, axisymmetric vortices are preferred. Moreover, the most energetic length-scale increases with time.

Of the host of properties and consequences detailed, possibly the most important are (i) the exact elementary solution (4), (ii) the lifetime expression (9), (iii) the vortex's trajectory, speed (16) and size (17), and (iv) the energy density variation (19) and consequent preferred length-scale (20). These have the power of explicitly expressing the dependence on the various parameters in the problem: the Coriolis parameter, the order of diffusivity, the magnitude of diffusivity, the geometry of the vortex, and the strength of the vortex. In different parameter regimes, appropriate expansions of these expressions could be used to determine dominant characteristics.

Many properties of the model examined herein are simplistic in comparison with experimental or some numerical data. For example, it is not possible to use specific structure characteristics of a vortex core, since (4) specifies this. Indeed, the eddies are *dipolar*, and it is not obvious whether they fall under the 'isolated' or 'non-isolated' classifications commonly used. Effects of baroclinicity, stratification, forcing and topography cannot be handled. Nevertheless, a possible rationalisation of the model is that it could be considered a first term in the spatial expansion (subject to dynamical consistency) of a locally isolated dipolar eddy's kinematic structure. Albeit with these idealisations, the model provides a wealth of formulas, and also quite easily establishes less obvious tendencies (such as the dichotomy in isotropy between large and small vortices). The model is also able to simultaneously handle *all* orders

of diffusivity, ranging from Rayleigh friction to super-diffusivity. There appears to be no qualitative difference in choosing different orders of diffusivity (beyond $n = 1$), which seems to support the variety of values used by numerical modellers.

The explicit formulas derived in this article were based on an elementary exact solution to the non-linear PV-dissipating equation. In the event that perturbations to this solution occur (say, through the creation of small eddies in the flow, or with using a more common form for the vorticity distribution in the vortex core), the basic geometrical structure of the eddy is expected to remain quite robust. Therefore, the expressions for its lifetime, meridional drift, size and energy density would only suffer perturbative changes. As such, the expressions and consequences derived in this paper should model primarily monochromatic vortices very well.

Acknowledgements

Thanks to Björn Sandstede, for his insight into the $n = 1$ case. Extensive discussions with (and suggestions from) Georg Gottwald and Charlie Macaskill are gratefully acknowledged. Detailed comments from an anonymous referee have added substantially to this article.

References

Adem, J., "A series solution for the barotropic vorticity equation and its application in the study of atmospheric vortices", *Tellus* **8**, 364–372 (1956).

Babiano, A., Bofetta, G., Provenzale, A. and Vulpiani, A., "Chaotic advection in point vortex models and two-dimensional turbulence", *Phys. Fluids* **6**, 2465–2474 (1994).

Baer, F., "An alternate scale representation of atmospheric energy spectra", *J. Atmos. Sci.* **29**, 649–664 (1972).

Balasuriya, S., "Vanishing viscosity in the barotropic β-plane", *J. Math. Anal. Appl.* **214**, 128–150 (1997).

Balasuriya, S., "Gradient evolution for potential vorticity flows", *Nonlin. Proc. Geophys.* **8**, 253–263 (2001).

Balasuriya, S. and Jones C.K.R.T., "Diffusive draining and growth of eddies", *Nonlin. Proc. Geophys.* **8**, 241–251 (2001).

Balasuriya, S., Jones, C.K.R.T. and Sandstede, B., "Viscous perturbations of vorticity conserving flows and separatrix splitting", *Nonlinearity* **11**, 47–77 (1998).

Basdevant, C., Legras, N., Sadourney, R. and Béland, M., "A study of barotropic model flows: intermittency, waves and predictability", *J. Atmos. Sci.* **38**, 2305–2326 (1981).

Carnevale, G.F., Kloosterziel, R.C. and van Heijst, G.J.F., "Propagation of barotropic vortices over topography in a rotating tank", *J. Fluid Mech.* **233**, 119–139 (1991).

Cushman-Roisin, B., *Introduction to Geophysical Fluid Dynamics*, Prentice Hall, New York (1994).

del Castillo-Negrete, D. and Morrison, P.J., "Chaotic transport by Rossby waves in shear flow", *Phys. Fluids A* **5**, 948–965 (1993).

Eliasen, E., "A study of long atmospheric waves on the basis of zonal harmonic analysis", *Tellus* **10**, 206–215 (1958).

Flierl, G.R., Malanotte-Rizzoli, P. and Zabusky, N.J., "Nonlinear waves and coherent vortex structures in barotropic β-plane jets", *J. Phys. Oceanography* **17**, 1408–1438 (1987).

Flór, J.-B. and Eames, I., "Dynamics of monopolar vortices on a topographic beta-plane", *J. Fluid Mech.* **456**, 353–376 (2002).

Gill, A.E., *Atmosphere-Ocean Dynamics*, Academic Press, New York (1982).

Haller, G. and Poje, A.C., "Eddy growth and mixing in mesoscale oceanographic flows", *Nonlin. Proc. Geophys.* **4**, 223–235 (1997).

Hopfinger, E.J. and van Heijst, G.J.F., "Vortices in rotating fluids", *Annu. Rev. Fluid Mech.* **25**, 241–289 (1993).

Kao, S.-K. and Wendell, L.L., "The kinetic energy of the large-scale atmospheric motion in wavenumber-frequency space: I. Northern hemisphere", *J. Atmos. Sci.* **27**, 359–375 (1970).

Kenyon, K., "Resonant interactions between planetary waves: discussion", *Proc. Roy. Soc. Lond.* A **299**, 141–144 (1967).

Knobloch, E. and Weiss, J.B., "Chaotic-advection by modulated travelling waves", *Phys. Rev. A* **36**, 1522–1524 (1987).
Korotaev, G.K. and Fedotov, A.B., "Dynamics of an isolated barotropic eddy on a beta-plane", *J. Fluid Mech.* **264**, 277–301 (1994).
Llewellyn Smith, S.G., "The motion of a non-isolated vortex on the beta-plane", *J. Fluid Mech.* **346**, 149–179 (1997).
Macaskill, C. and Bewick, B.M., "The use of hyperviscosity in simulations of nonlinear geophysical fluid flows", *Proceedings of the Twelfth Australian Fluid Mechanics Conference*, 415–418 (1995).
Marcus, P.S. and Lee, C., "Jupiter's Great Red Spot and zonal winds as a self-consistent, one-layer, quasigeostrophic model", *Chaos* **4**, 269–286 (1994).
Masuda, A., Marubayashi, K. and Ishibashi, M., "A laboratory experiment and numerical simulation of an isolated barotropic eddy in a basin with topographic β", *J. Fluid Mech.* **213**, 641–655 (1990).
McWilliams, J.C., "The emergence of isolated coherent vortices in turbulent flow", *J. Fluid Mech.* **146**, 21–42 (1984).
McWilliams, J.C., "The vortices of two-dimensional turbulence", *J. Fluid Mech.* **219**, 361–385 (1990).
McWilliams, J.C. and Flierl, G.R., "On the evolution of isolated, nonlinear vortices", *J. Phys. Oceanography* **9**, 1155–1182 (1979).
Meyers, S.D., "Cross-frontal mixing in a meandering jet", *J. Phys. Oceanography* **24**, 1641–1646 (1994).
Miller, P., Jones, C.K.R.T., Rogerson, A.M. and Pratt, L.J., "Quantifying transport in numerically generated vector fields", *Physica D* **110**, 105–122 (1997).
Nezlin, M.V. and Snezhkin, E.N., *Rossby Vortices, Spiral Structures, Solitons*, Springer-Verlag, Berlin (1993).
Pedlosky, J., *Geophysical Fluid Dynamics*, Springer (1979).
Pierrehumbert, R.T., "Chaotic mixing of tracer and vorticity by modulated traveling Rossby waves", *Geophys. Astrophys. Fluid Dynam.* **58**, 285–319 (1991).
Poje, A.C., Haller, G. and Mezić, I., "The geometry and statistics of mixing in aperiodic flows", *Phys. Fluids* **11**, 2963–2968 (1999).
Pratt, L.J., Lozier, M.S. and Beliakova, N., "Parcel trajectories in quasigeostrophic jet: normal modes", *J. Phys. Oceanography* **25**, 1451–1466 (1995).
Provenzale, A., "Transport by coherent barotropic vortices", *Annu. Rev. Fluid Mech.* **31**, 55–93 (1999).
Reznik, G.M., "Dynamics of singular vortices on a beta-plane", *J. Fluid Mech.* **240**, 405–432 (1992).
Reznik, G.M. and Dewar, W.K., "An analytical theory of distributed axisymmetric brotropic vortices on the β-plane", *J. Fluid Mech.* **269**, 301–321 (1994).
Rhines, P.B., "Waves and turbulence on a beta-plane", *J. Fluid Mech.* **69**, 417–443 (1975).
Richardson, P.L., "Gulf Stream Rings". In: *Eddies in Marine Science* (Ed. Robinson, A.R.) pp. 19–45, Springer-Verlag, Berlin (1983).
Rogerson, A.M., Miller, P.D., Pratt, L.J. and Jones, C.K.R.T., "Lagrangian motion and fluid exchange in a barotropic meandering jet", *J. Phys. Oceanography* **29**, 2635–2655 (1999).
Rossby, C.-G., "On displacements and intensity changes of atmospheric vortices", *J. Marine Res.* **7**, 175–187 (1948).
Samelson, R.M., "Fluid exchange across a meandering jet", *J. Phys. Oceanography* **22**, 431–444 (1992).
Sandstede, B., Balasuriya, S. and Jones, C.K.R.T., "Melnikov theory for finite-time vector fields", *Nonlinearity* **13**, 1357–1377 (2000).
Smith, R.K. and Ulrich, W., "An analytical theory of tropical cyclone motion using a barotropic model", *J. Atmos. Sci.* **47**, 1973–1986 (1990).
Stegner, A. and Zeitlin, V., "From quasi-geostrophic to strongly nonlinear monopolar vortices in a paraboloidal shallow-water-layer experiment", *J. Fluid Mech.* **356**, 1–24 (1998).
Sutyrin, G.G., Hesthaven, J.S., Lynov, J.P. and Rasmussen, J.J., "Dynamical properties of vortical structures on the beta-plane", *J. Fluid Mech.* **268**, 103–131 (1994).
van Heijst, G.J.F. and Clercx, H.J.H., "Self-organisation is quasi-2D flows in a rectangular container", *Appl. Sci. Res.* **58**, 149–168 (1998).
Wajsowicz, R.C., "Free planetary waves in finite-difference numerical models", *J. Phys. Oceanography* **16**, 773–789 (1986).
Weiss, J.B., "Hamiltonian maps and transport in structured fluids", *Physica D* **76**, 230–238 (1994).
Weiss, J.B. and Knobloch, E., "Mass transport and mixing by modulated traveling waves", *Phys. Rev. A* **40**, 2579–2589 (1989).
Wiggins, S., *Global Bifurcations and Chaos*, Spinger, New York (1988).
Williams, G.P. and Yamagata, T., "Geostrophic regimes, intermediate solitary vortices and Jovian eddies", *J. Atmos. Sci.* **41**, 453–478 (1984).
Willoughby, H.E., "Linear motion of a shallow-water barotropic vortex", *J. Atmos. Sci.* **45**, 1906–1928 (1989).
Yuan, G.-C., Pratt, L.J. and Jones, C.K.R.T., "Barrier destruction and Lagrangian predictability at depth in a meandering jet", *Dyn. Atmos. Oceans* **35**, 41–61 (2002).